Journal of Magnetic Resonance **136,** 69–75 (1999)
Article ID jmre.1998.1617, available online at http://www.idealibrary.com on IDEAL®

Reference Deconvolution in the Frequency Domain

Martin Goez and Rainer Heun

Fachbereich Chemie, Martin-Luther-Universität Halle–Wittenberg, Kurt-Mothes-Strasse 2, D-06120 Halle/Saale, Federal Republic of Germany

E-mail: goez@chemie.uni-halle.de

Received June 8, 1998; revised September 15, 1998

Reference deconvolution, i.e., using the lineshape distortions of a reference signal with known ideal shape to deduce a correction function for the whole spectrum, is normally performed in the time domain. As a disadvantage, reference signals of higher multiplicity cannot be employed because of mathematical instabilities. In this work we show that these difficulties can be circumvented by carrying out reference deconvolution in the frequency domain. The computational demands of this approach are higher, but not prohibitive, because the width of the correction function is only a fraction of that of the whole spectrum. An iterative algorithm was implemented that yields the optimum widths of the correction function and of the ideal reference signal. Singular value decomposition was found to produce better results than *LU* decomposition of the design matrix. The feasibility of the deconvolution method and of the algorithm are demonstrated using both synthetic and experimental data. © 1999 Academic Press

Key Words: **NMR spectroscopy; spectrum processing; frequency domain methods; resolution enhancement; reference deconvolution.**

INTRODUCTION

Every experimental NMR spectrum is a convolution of the ideal spectrum with the response function of the spectrometer. The resulting changes of lineshapes, intensities, and positions can make evaluation difficult and lead to wrong predictions of spectral or kinetic parameters. For most kinds of instrumental imperfections, above all inhomogeneity of B_0, the response function is independent of frequency and thus affects all signals of the spectrum in the same way. The resulting errors can be eliminated by reference deconvolution. This technique relies on a signal for which the ideal shape is known. From the form of this reference signal in the experimental spectrum, a correction function is derived and then applied to the whole spectrum. Since its first application to NMR difference spectroscopy in 1977 (*1*), reference deconvolution has found widespread use in different branches of high-resolution NMR (*2–4*), in particular NOE difference measurements (*5*), 2D NMR experiments (*6*) including pulsed-field-gradient methods (*7*), and dynamic NMR spectroscopy with total band shape analysis (*8*).

In all cases reported in the NMR literature so far, reference deconvolution has been performed in the time domain only. Computationally, this is extremely efficient because it simply amounts to point-by-point multiplication and division of free induction decays. However, when the reference signal possesses a multiplet structure and its free induction decay therefore passes through zero, numerical instabilities can arise. This limits the applicability of reference deconvolution because very often the spectrum does not contain a suitable singlet peak. Although the addition to the sample of a substance yielding such a signal can solve this problem, it is frequently undesirable (e.g., when the sample is needed for other experiments and the reference substance must thus be removed again, or because of possible interactions between the reference substance and other species in the sample) or even impossible (e.g., in the case of *in vivo* NMR).

In this work, we investigate reference deconvolution in the frequency domain. This method is better conditioned mathematically, though somewhat more demanding computationally. However, the computational effort is not as large as it may seem at first glance: under usual conditions the response function is confined to a fairly narrow frequency interval, so in order to correct a given data point, only a small number of points in its vicinity must be considered. The main advantage of this approach is that it allows multiplets (for instance, the ubiquituous solvent peak, which is a multiplet for quite a number of common solvents) to be used as reference signals. This should considerably increase the range of applicability of reference deconvolution.

RESULTS AND DISCUSSION

Deconvolution in the Time and Frequency Domains

The experimental spectrum in the frequency domain $S_{\mathrm{exp}}(\omega)$ is given by the convolution of the ideal spectrum $S_{\mathrm{id}}(\omega)$ with the instrumental response $R(\omega)$,

$$S_{\mathrm{exp}}(\omega) = \int_{-\infty}^{+\infty} S_{\mathrm{id}}(\omega')\, R(\omega - \omega')\, d\omega'. \qquad [1]$$

According to the reciprocity theorems of Fourier transforma-

1090-7807/99 $30.00

tion, Eq. [1] is equivalent to multiplication of the ideal free induction decay $S_{id}(t)$ (for simplicity, we use the same symbol for a time-domain function and its corresponding frequency-domain function, and distinguish between them by explicitly giving the variable t or ω) with the Fourier transform $R(t)$ of the instrumental response,

$$S_{exp}(t) = S_{id}(t) \cdot R(t). \quad [2]$$

From Eq. [2], it is immediately obvious that the ideal time-domain signal can be recovered by multiplying the experimental free induction decay by $1/R(t)$. By the same token, the ideal spectrum is regained by a convolution of the experimental spectrum with the Fourier transform of $1/R(t)$:

$$S_{id}(t) = \frac{S_{exp}(t)}{R(t)} \quad [3]$$

$$S_{id}(\omega) = \int_{-\infty}^{+\infty} S_{exp}(\omega')C(\omega - \omega')d\omega' \quad [4]$$

$$C(\omega) = \mathcal{FT}\left(\frac{1}{R(t)}\right). \quad [5]$$

The implementation of reference deconvolution in the time domain (free-induction-decay deconvolution for lineshape enhancement, FIDDLE) is well documented (*2–4*): $S_{exp}(t)$ is zero-filled to twice its length and Fourier transformed. Phase and baseline of the spectrum $S_{exp}(\omega)$ are corrected. The imaginary part of $S_{exp}(\omega)$ as well as all signals of the real part except the reference peak are set to zero, i.e., only the absorption mode of the reference signal is retained. Inverse Fourier transformation and discarding the second half of the resulting symmetrical free induction decay yield the experimental reference signal $S_{ref,exp}(t)$. The ideal reference signal $S_{ref,id}(t)$ is constructed either directly in the time domain or in the frequency domain with subsequent inverse Fourier transformation. The corrected time-domain signal $S_{corr}(t)$ is finally obtained by

$$S_{corr}(t) = \frac{S_{ref,id}(t)}{S_{ref,exp}(t)} S_{exp}(t). \quad [6]$$

When a singlet is used as the reference signal, this procedure is well-conditioned mathematically, but reference signals possessing a multiplet structure lead to zeroes in the time domain. At these points of time, the free induction decay does not contain any information about the deviations of the experimental signal from the ideal signal. In a hypothetical noise-free experiment, numerator and denominator of the fraction $S_{ref,id}(t)/S_{ref,exp}(t)$ become zero simultaneously, and the resulting indeterminate expressions can be resolved mathematically. In the presence of noise, however, spikes arise, and the "corrected" spectrum does not deserve the epithet.

In the frequency domain, an n-fold multiplet can be obtained by convolution of a singlet with n δ-functions separated by the coupling constant J. In the time domain, this is equivalent to a multiplication of the free induction decay by $\cos^n(\pi Jt)$. As Bothner-By and Dadok (*9*) suggested, the multiplet structure of the reference peak can therefore be eliminated by multiplying the free induction decay by $1/\cos^n(\pi Jt)$. However, this causes essentially the same mathematical difficulties. On the one hand, in the vicinity of the zero crossings of the cosine term information must be extracted from data points of the free induction decay that lie below the noise level. On the other hand, any uncertainty in the preacquisition delay leads to a shift of the zero crossings of the experimental time-domain signal versus those of $\cos^n(\pi Jt)$, and thus to spikes.

The approach of Morris *et al.* (*10*) is based on interpolation over the gaps of the time-domain correction function $C(t)$ and demands careful iterative determination of estimates for the coupling constant, chemical shift, signal asymmetry, and preacquisition delay. As these authors pointed out, the applicability of their algorithm is limited to doublet signals. With reference signals of higher multiplicity, the free induction decay often possesses much broader regions in the vicinity of the zero crossings where it falls below the noise level, so the interpolation must be performed over a range that is too wide for satisfactory results.

Evidently, the origin of the stability problems with deconvolution in the time domain is the fact that each data point of the correction function $C(t)$ is obtained from exactly one data point of the free induction decay, so precise results for $C(t)$ cannot be expected wherever the time-domain signal does not contain sufficient information about the instrumental response, i.e., wherever the ideal signal is near zero. In contrast, with deconvolution in the frequency domain each data point of the correction function $C(\omega)$ is determined from a series of data points of the spectrum, thus avoiding this difficulty.

In the strict mathematical sense, the stability problem is not eliminated completely by this approach because situations could arise where $C(\omega)$ does not exist or is not unique (*11*). This, however, would imply that $C(t)$ cannot be Fourier transformed, so in these pathological cases deconvolution in the time domain would be unlikely to succeed, either. Apart from this rather theoretical limitation, the computational demands are certainly higher when deconvolution is performed in the frequency domain, although this constitutes no fundamental handicap (the more so when one considers the present trends in hardware speed and prices); besides, it is normally sufficient to employ a correction function that is only a fraction of the size of the whole spectrum, e.g., a few hundreds of data points. As a further consequence, the reference signal does not need to lie completely isolated from other signals of the spectrum, as opposed to time-domain deconvolution where inverse Fourier transformation of $S_{exp}(\omega)$ produces artifacts unless the absorp-

tion-mode signal of the reference decays to a low level within the spectral window chosen (compare the above description of the FIDDLE algorithm).

Determination of the Correction Function

For a discrete deconvolution of an experimental spectrum $S_i^{\exp}$ with the correction function C_j, both of which possess a finite definition range, Eq. [4] is transformed into

$$S_k^{\text{corr}} = \sum_{i=k-n}^{k+n} S_i^{\exp} \cdot C_{k-i}, \qquad [7]$$

where S_k^{corr} is the corrected spectrum. An analogous equation holds for the relationship between the experimental reference signal X_i and the ideal reference signal R_k, the correction function being the same as in Eq. [7],

$$R_k = \sum_{i=k-n}^{k+n} X_i \cdot C_{k-i}. \qquad [8]$$

Let the width of the ideal reference signal be m data points. From the preceding equations, the width of the correction function is seen to be $2n + 1$ data points. The corrected spectrum is thus shorter than the experimental one by n data points at either end, and an interval of $m + 2n + 1$ data points of the experimental reference signal is needed to determine the correction function.

To avoid zero or negative indices, the discrete functions X and C are replaced by x and c, the correspondences being given by

$$X_p \leftrightarrow x_{p+n}$$
$$C_q \leftrightarrow c_{n+1-q}.$$

With these new variables, the system of linear equations following from Eq. [8] is written in matrix notation as

$$\mathbf{r} = \mathbf{X} \cdot \mathbf{c}$$

$$\begin{pmatrix} R_1 \\ R_2 \\ \vdots \\ R_m \end{pmatrix} = \begin{pmatrix} x_1 & x_2 & \cdots & x_{2n+1} \\ x_2 & x_3 & \cdots & x_{2n+2} \\ \vdots & \vdots & \ddots & \vdots \\ x_m & x_{m+1} & \cdots & x_{2n+m} \end{pmatrix} \cdot \begin{pmatrix} c_1 \\ c_2 \\ \vdots \\ c_{2n+1} \end{pmatrix}. \qquad [9]$$

For $m < 2n + 1$, i.e., when the width of the correction function is larger than the width of the ideal reference signal, the system of linear equations, Eq. [9], is underdetermined. When $m = 2n + 1$, the matrix $\mathbf{X}$ is square, and one solution exists unless $\mathbf{X}$ is singular. In the usual case of $m > 2n + 1$, however, the system is overdetermined. Under these conditions, an optimum solution can be sought that minimizes χ^2,

$$\chi^2 = (\mathbf{X} \cdot \mathbf{c} - \mathbf{r})^2. \qquad [10]$$

An iterative procedure was used to obtain the correction function:

1. The optimum (in the sense of Eq. [10]) solution vector of Eq. [9] is calculated for given m and n and for an ideal reference signal constructed from a given set of spectral parameters P_l.
2. Several of the P_l (e.g., the chemical shift, which depends on temperature and often on the composition of the sample) cannot be predicted accurately enough, so these are treated as free parameters. The same holds for m and n because increasing their values increases the information about the line distortions, but in a real spectrum also increases the noise.

This sequence is repeated until a minimum of χ^2 is reached, and $\mathbf{c}$ thus constitutes the optimum correction function.

For the minimization, a simplex algorithm was employed because this does not need derivatives and allows easy implementation of the condition that $2n + 1$ must be smaller than m. The program code for this subroutine, as well as for the others described below, was taken from Ref. (*12*). To maintain the nondegeneracy of the simplex, continuous variables were used for the width of the ideal reference signal and that of the correction function, and these were mapped onto the discrete variables m and n for each calculation of χ^2.

Step 1 of the above procedure was carried out either by using the normal equations and LU decomposition, or by singular value decomposition. With the first method, Eq. [9] is multiplied from the left with the transpose of **X,**

$$\mathbf{X}^T \cdot \mathbf{r} = \mathbf{X}^T\mathbf{X} \cdot \mathbf{c}. \qquad [11]$$

This reduces the dimension of the vector on the left-hand side from m to $2n + 1$; however, $\mathbf{X}^T \cdot \mathbf{r}$ still contains information on all m data points of the ideal reference signal **r.** Likewise, the rectangular matrix $\mathbf{X}$ of dimension $(2n + 1) \times m$ is transformed into a $(2n + 1) \times (2n + 1)$ square matrix $\mathbf{X}^T\mathbf{X}$, which takes less storage. The elements of the so-called design matrix $\mathbf{X}^T\mathbf{X}$ are given by

$$(\mathbf{X}^T\mathbf{X})_{ij} = \sum_{k=0}^{m-1} x_{i+k} \cdot x_{j+k}. \qquad [12]$$

It is evident that $\mathbf{X}^T\mathbf{X}$ is symmetrical and can be constructed in a straightforward way from the experimental spectrum. The set of normal equations, Eq. [11], solves the linear least squares problem, as can be shown by differentiation of Eq. [10] (*12*).

Equation [11] is then solved by LU decomposition (*12*), i.e.,

by determining a lower triangular matrix **L** (nonzero elements only on the diagonal and below) and an upper triangular matrix **U** (nonzero elements only on the diagonal and above) such that

$$\mathbf{X}^T\mathbf{X} = \mathbf{LU}. \quad [13]$$

Compared to other methods for the solution of systems of linear equations, e.g., Gauss–Jordan elimination, *LU* decomposition is faster and more stable against round-off error. However, its main advantage is that once the *LU* decomposition of $\mathbf{X}^T\mathbf{X}$ has been found, which requires on the order of n^3 multiplications, the solution for a given vector $\mathbf{X}^T \cdot \mathbf{r}$ can be obtained by an n^2 process (a forward–backward substitution scheme). This allowed a much more efficient optimization of the parameters because it was generally found that in the later stages of the iteration procedure m and n tend to remain constant, so the design matrix $\mathbf{X}^T\mathbf{X}$ (and thus its *LU* decomposition) does not change.

The second method is singular value decomposition (*12*) of the $(2n + 1) \times m$ matrix **X.** With this algorithm, a $(2n + 1) \times m$ column orthogonal matrix **U,** a $(2n + 1) \times (2n + 1)$ diagonal matrix diag(w_j), and a $(2n + 1) \times (2n + 1)$ orthogonal matrix **V** are determined such that

$$\mathbf{X} = \mathbf{U} \cdot \mathrm{diag}(w_j) \cdot \mathbf{V}^T. \quad [14]$$

Because of the special properties of these matrices, the least square solution vector **c** is then given by (*12*)

$$\mathbf{c} = \mathbf{V} \cdot \mathrm{diag}(1/w_j) \cdot \mathbf{U}^T \cdot \mathbf{r}. \quad [15]$$

The operational count of singular value decomposition is only slightly higher than that of *LU* decomposition. Again, once the decomposition is known, the solution for a given vector **r** is much less costly, so optimization of the parameters can again be implemented efficiently. Singular value decomposition is an exceptionally stable procedure that can even be applied when the matrix is singular. In this case, the algorithm separately yields orthonormal bases for the range and the nullspace of the matrix, and these can be combined in a very simple way to find the solution vector of the smallest length (*12*): Any singularity is reflected by a zero element w_j, and the desired solution vector is found by zeroing the associated element $1/w_j$ in Eq. [15]. In the presence of noise, the matrix can be numerically close to singular. In this case, one or more elements w_j become very small. As this corresponds to an ambiguous combination of input data, *LU* decomposition yields a strongly oscillating solution vector under these circumstances, and better results are obtained with singular value decomposition because the pertaining combination of variables can be discarded by setting the reciprocal element $1/w_j$ equal to zero.

It is obvious that the optimization will proceed faster the better the starting values of the spectral parameters P_l are. Furthermore, because of the strong dependence of the *LU* or singular value decompositions on the width of the correction function, it is computationally much more efficient to start the iterations with a small width and let the simplex algorithm enlarge it than to approach the optimum width from the other side.

Before the calculations, phase and baseline of the spectra were carefully corrected. Only data from the real part of the spectrum (absorption mode) were used for the determination of the correction function, i.e., as the experimental reference signal X_i. The reason is that with a Lorentzian line the absorption and dispersion mode signals decay asymptotically as $1/(\omega - \omega_0)^2$ and $1/(\omega - \omega_0)$, respectively. Although a truncation of the dispersion mode signal would not cause problems with deconvolution in the frequency domain—as opposed to deconvolution in the time domain, where inverse Fourier transformation of the truncated signal would give rise to severe artifacts, and where the imaginary part must therefore be discarded (*4*)—the tail of the dispersive flank of a nearby signal would corrupt X_i, because this has the same effect as a strongly distorted baseline.

In this paper, only reference signals characterized by a single resonance frequency and a single coupling constant (typically the quintet of a CHD_2 group, as in deuterated acetonitrile, methanol, or acetone) were used. No new aspects arise when more complicated cases are considered. Spectral parameters P_l were the residual offset of the baseline, as well as J, ω_0, and T_2 of the reference signal. Only the first two parameters were made adjustable, whereas ω_0 was extracted from X_i, and for T_2 the value obtained from a well-shimmed spectrum was used. The reasons for this choice are that a baseline offset can be compensated much more easily by an additive algorithm than by a multiplicative one (Eq. [7]), and that an error in the coupling constant induces a frequency-dependent deviation, which would be at variance with the fundamental premise of reference deconvolution. In contrast to this, slight inaccuracies in ω_0 or T_2 do not have a crucial effect on the corrected spectrum. The former leads only to a small shift of the whole spectrum, and the latter is equivalent to a multiplication of the free induction decay by $\exp(t/T_{2,\mathrm{true}} - t/T_2)$; as the value assumed for T_2 will usually be too long rather than too short, line narrowing accompanied by a decrease of the signal-to-noise ratio results, but unless T_2 is unreasonably short, this will not cause any stability problems.

Examples

The algorithm was tested with both synthetic and experimental data.

Figure 1 shows an example with synthetic data and fairly high digital resolution (0.046 Hz per data point). As signal and reference, an ABCD spin system ($T_2^{\mathrm{sig}} = 1.5$ s) and a quintet ($T_2^{\mathrm{ref}} = 1.0$ s) with the spectral parameters of CD_3CN were

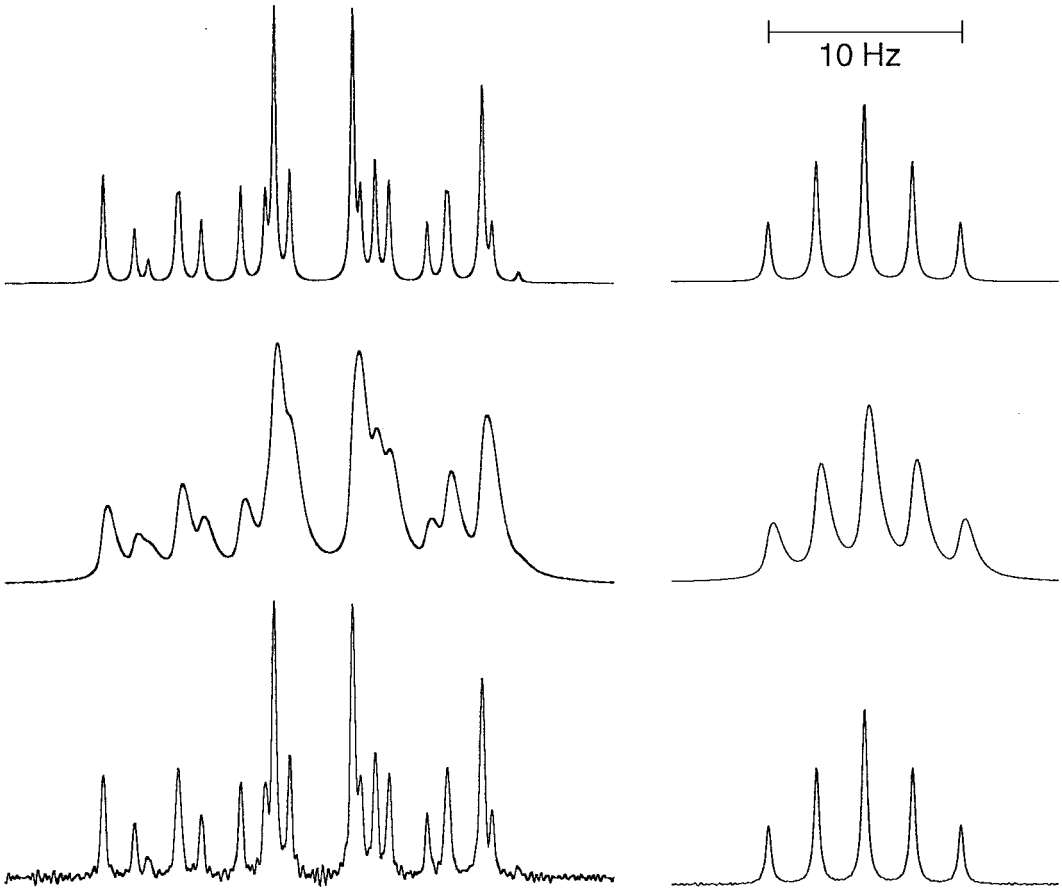

FIG. 1. Test of the deconvolution algorithm with synthetic data. Left, signal of an ABCD spin system; right, quintet reference signal. Top trace, ideal spectrum; center trace, after convolution with an asymmetric line broadening function and addition of noise; bottom trace, after deconvolution. For further explanation, see text.

chosen. For simplicity, the maximum peak intensities of signal and reference were taken to be comparable. The ideal spectrum is displayed at the top of the figure.

An asymmetrical line broadening function was constructed as the sum of 10 Gaussians of different amplitudes, linewidths, and center positions within an interval of 0.5 Hz. Convolution of the ideal spectrum with this line broadening function and superposition of statistical noise (signal-to-noise ratio 4000:1) yielded the spectrum shown as the center trace of the figure. The signals are broadened considerably ($T_2^{\text{add}} \approx 0.45$ s); they exhibit a pronounced asymmetry, and the small couplings are no longer resolved.

This spectrum served as the input to the deconvolution procedure. For T_2 of the reference signal, we took the value of the ideal spectrum, which is a rather strict condition. Starting parameters for the iterations were $J = 2.55$ Hz (as estimated from the broadened spectrum), a baseline offset of zero, a width of the correction function of 2.62 Hz (57 data points), and a width of the ideal reference signal of 16.88 Hz (368 data points). The iterations converged on $J = 2.48953$ Hz, which differs from the value of the ideal spectrum by 0.00053 Hz (i.e., two orders of magnitude below the digital resolution), a baseline offset of 0.013% of the peak height instead of zero, and widths of the correction function and the ideal reference signal of 6.12 and 17.71 Hz, respectively. With these final parameters, χ^2 was 50 times lower than with the starting set.

The bottom trace of the figure displays the spectrum after deconvolution with the correction function obtained by singular value decomposition, where only elements w_j of magnitude greater than 10^{-8} of the maximum value were retained (this amounted to three-quarters of the w_j), and $1/w_j$ was set to zero for the others. The peaks are seen to be sharp and symmetrical, and the small couplings are well resolved again. Using the ABCD signal, after deconvolution, as the input to LAOCOON (*14*) gave spectral parameters that were essentially identical to those initially used, whereas determination of several of these parameters is impossible with the spectrum in the center trace.

It is evident that deconvolution must decrease the signal-to-noise ratio. In the example shown, this effect is particularly pronounced (the signal-to-noise ratio after deconvolution is about 80, i.e., worse by a factor of 50 than in the spectrum before deconvolution). This, however, is not due to the fact that

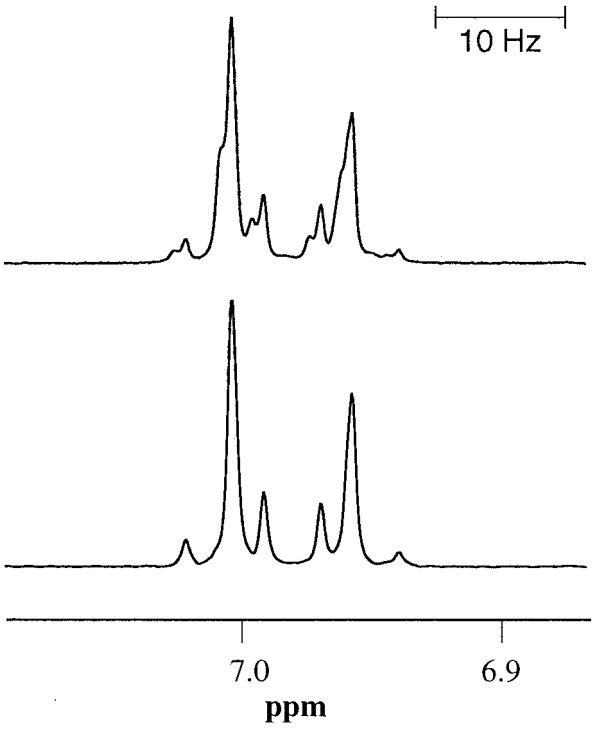

FIG. 2. Application of the deconvolution algorithm to an experimental spectrum (dynamic NMR spectrum of *p*-methoxy-*N*,*N*-dimethylaniline and its conjugated acid in acetonitrile-d_3) measured on a Varian Gemini 200 spectrometer. Shown is the signal of the meta protons of the substrate only. Top, spectrum obtained with misadjusted shims; bottom, after deconvolution. For further explanation, see text.

the deconvolution is performed in the frequency domain instead of the time domain; rather, the reason is the considerable degree of line broadening that is undone. When the spectrum before deconvolution (center of Fig. 1) is Fourier transformed and an exponential multiplication is applied to recover the initial linewidths, a comparable deterioration of the signal-to-noise ratio occurs.

Iterative adjustment of the P_l, m, and n was found to be very important. Missettings of J by as little as 0.01 Hz already led to noticeable distortions of the baseline. Distortions also arise when the width of the correction function or that of the ideal reference signal are changed. As long as the ratio of m and $(2n + 1)$ is kept constant, these effects are not very severe. However, when this ratio was decreased by 50%, the baseline artifacts became so strong that the spectrum was no longer discernible.

It is clear that in a noise-free spectrum LU decomposition and singular value decomposition are equivalent as long as the matrix is not singular and round-off errors can be neglected. In this ideal case, there is also no point in zeroing certain elements $1/w_j$ because all of the associated data contain relevant information. However, in the presence of noise, singular value decomposition together with zeroing those elements $1/w_j$ that indicate ambiguous combinations of input data generally gave results that were superior to those of LU decomposition, in the sense that the baseline artifacts were considerably smaller.

A universal rule for the cutoff limit of the w_j cannot be given. Plotting $\log(w_j)$ sorted by size is a helpful though somewhat time-consuming procedure. The distribution of the w_j depends on the (usually unknown) shape of the line broadening function and on the signal-to-noise ratio. It seems natural to assume that for a constant line broadening function one should select a cutoff limit of the w_j that is inversely proportional to the signal-to-noise ratio.

Finally, the applicability of the described algorithm is also demonstrated with an experimental spectrum. A dynamic NMR measurement was chosen for this purpose because with this method lineshape distortions are especially problematic and lead to wrong estimates of the kinetic parameters. By reference deconvolution one can easily correct for varying field homogeneity between the spectra of a series. In this way the hypothetical static signals for the sample under study can be obtained very accurately and reliably from nonexchanging reference samples, and the shimming procedure can be shortened considerably.

Portions of the dynamic NMR spectra (digital resolution 0.11 Hz per data point) observed in proton self-exchange between *p*-methoxy-*N*,*N*-dimethylaniline and its conjugated acid (*13*) are shown in Fig. 2. The reference signal was again the quintet of CD_3CN. The spectrum was recorded with the shims deliberately misadjusted. The resulting artifacts (a shoulder at half height, which even gives rise to a signal splitting with the smaller peaks) are clearly discernible.

The iterations were started with $J = 2.55$ Hz, width of the correction function 6.26 Hz (57 data points), width of the ideal reference signal 40.43 Hz (368 data points), and baseline offset zero. T_2 of the ideal reference signal was taken to be 0.65 s. The final values of the parameters were $J = 2.47122$ Hz, widths of the correction function and the ideal reference signal 10.44 and 22.41 Hz (95 and 204 data points), respectively, and an offset of 0.011% of the peak height. Again, singular value

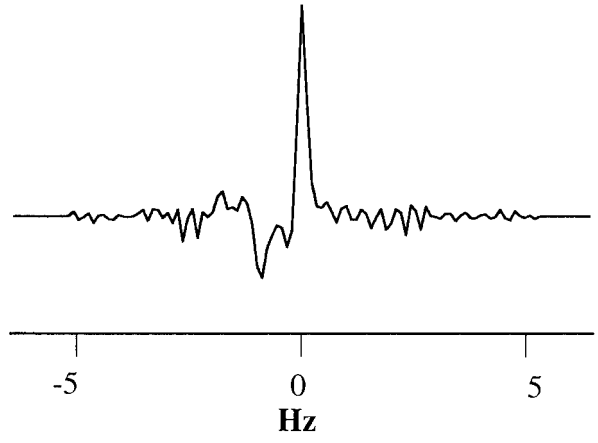

FIG. 3. Correction function employed for deconvolution in Fig. 2.

decomposition gave better results than LU decomposition. Four-fifths of the w_j were retained, the cutoff limit being set to 10^{-5} of the maximum w_j. The correction function has been plotted in Fig. 3.

The bottom trace of Fig. 2 displays the corrected signals. It is seen that the shoulders and splittings are no longer present; the lineshape is Lorentzian, and there are no baseline artifacts. Applying the program DNMR5 (*15*) to the corrected spectrum and to the uncorrected one gave exchange rates that differed by a factor of 1.35. This example further shows that in a realistic case, i.e., in the absence of excessive line broadening by instrumental imperfections, the loss of sensitivity (signal-to-noise ratio before deconvolution 400:1, after deconvolution 350:1) and the baseline distortions are much smaller than in the previous instance (Fig. 1), where synthetic data were used.

CONCLUSIONS

The feasibility of reference deconvolution in the frequency domain has been demonstrated. With this approach, reference signals of arbitrary multiplicity can be used, which is not possible when reference deconvolution is performed in the time domain. This should broaden considerably the applicability of reference deconvolution. The computational demands of deconvolution in the frequency domain are certainly higher than with the FIDDLE algorithm, but in the age of powerful personal computers this is no longer a true limitation.

REFERENCES

1. (a) J. M. Wouters and G. A. Petersson, Reference lineshape adjusted difference NMR spectroscopy. I. Theory, *J. Magn. Reson.* **28,** 81–91 (1977); (b) J. M. Wouters, G. A. Petersson, W. C. Agosta, F. H. Field, W. A. Gibbons, H. Wyssbrod, and D. Cowburn, Reference lineshape adjusted difference NMR spectroscopy. II. Experimental verification, *J. Magn. Reson.* **28,** 93–104 (1977).
2. J. Taquin, Line-shape and resolution enhancement of high-resolution F.T.N.M.R. in an inhomogeneous magnetic field, *Rev. Phys. Appl.* **14,** 669–681 (1979).
3. G. A. Morris, Compensation of instrumental imperfections by deconvolution using an internal reference signal, *J. Magn. Reson.* **80,** 547–552 (1988).
4. A. Gibbs and G. A. Morris, Reference deconvolution. Elimination of distortions arising from reference line truncation, *J. Magn. Reson.* **91,** 77–83 (1991).
5. G. A. Morris and D. Cowburn, Suppression of artefacts in nuclear Overhauser effect difference spectroscopy by reference deconvolution, *Magn. Reson. Chem.* **27,** 1085–1089 (1989).
6. A. Gibbs, G. A. Morris, A. G. Swanson, and D. Cowburn, Suppression of t_1 noise in 2D NMR spectroscopy by reference deconvolution, *J. Magn. Reson. A* **101,** 351–356 (1993).
7. H. Barjat, G. A. Morris, S. Smart, A. G. Swanson, and S. C. R. Williams, High-resolution diffusion-ordered 2D spectroscopy (HR-DOSY)—a new tool for the analysis of complex mixtures, *J. Magn. Reson. B* **108,** 170–172 (1995).
8. D. V. S. Green, I. H. Hillier, G. A. Morris, and L. Whalley, Determination of the barrier to C–N bond rotation in captopril: Application of reference deconvolution for lineshape analysis, *Magn. Reson. Chem.* **28,** 820–823 (1990).
9. A. A. Bothner-By and J. Dadok, Useful manipulations of the free induction decay, *J. Magn. Reson.* **72,** 540–543 (1987).
10. H. Barjat, G. A. Morris, A. G. Swanson, S. Smart, and S. C. R. Williams, Reference deconvolution using multiplet reference signals, *J. Magn. Reson. A* **116,** 206–214 (1995).
11. Y. G. Biraud, Les methodes de deconvolution et leurs limitations fondamentales, *Rev. Phys. Appl.* **11,** 203–214 (1976).
12. W. H. Press, B. P. Flannery, S. A. Teukolsky, and W. T. Vetterling, "Numerical Recipes. The Art of Scientific Computing," Cambridge Univ. Press, Cambridge (1986).
13. M. Goez and R. Heun, Proton self-exchange of *para*-substituted *N,N*-dimethylanilines and their conjugate acids in aprotic solvents, *Ber. Bunsenges. Phys. Chem.* **102,** 560–566 (1998).
14. Program LAOCN-5 (QCPE 458) by L. Cassidei and O. Sciacovelli.
15. Program DNMR5 (QCPE 569) by D. S. Stephenson and G. Binsch.